


# Similarities and differences in metabolites of tongue cancer cells among two- and three-dimensional cultures and xenografts

Shoko Murakami<sup>1,2</sup> | Hiroyuki Tanaka<sup>3</sup> | Takahisa Nakayama<sup>1</sup> | Naoko Taniura<sup>1</sup> | Toru Miyake<sup>4</sup> | Masaji Tani<sup>4</sup> | Ryoji Kushima<sup>1,5</sup> | Gaku Yamamoto<sup>2</sup> | Hiroyuki Sugihara<sup>1</sup> | Ken-ichi Mukaisho<sup>1</sup> 

<sup>1</sup>Division of Human Pathology, Department of Pathology, Shiga University of Medical Science, Otsu, Japan

<sup>2</sup>Department of Oral and Maxillofacial Surgery, Shiga University of Medical Science, Otsu, Japan

<sup>3</sup>Department of Biochemistry and Molecular Biology, Shiga University of Medical Science, Otsu, Japan

<sup>4</sup>Department of Surgery, Shiga University of Medical Science, Otsu, Japan

<sup>5</sup>Division of Clinical Laboratory Medicine, Shiga University of Medical Science, Otsu, Japan

## Correspondence

Ken-ichi Mukaisho, Division of Human Pathology, Department of Pathology, Shiga University of Medical Science, Seta-tsukinowa-cho, Otsu, Shiga 520-2192, Japan.  
Email: mukaisho@belle.shiga-med.ac.jp

## Abstract

Metabolic programming of cancer cells is an essential step in transformation and tumor growth. We established two-dimensional (2D) monolayer and three-dimensional (3D) cultures, the latter called a “tissueoid cell culture system”, using four types of tongue cancer cell lines. We also undertook a comprehensive metabolome analysis of three groups that included xenografts created by transplanting the cell lines into nude mice. In addition, we undertook a functional analysis of the mitochondria, which plays a key role in cancer metabolism. Principal component analysis revealed the plots of the four cell lines to be much narrower in 2D culture than in 3D culture and xenograft groups. Moreover, compared to xenografts, the 2D culture had significantly lower levels of most metabolites. These results suggest that the unique characteristics of each cell disappeared in 2D culture, and a type of metabolism unique to monolayer culture took over. Conversely, ATP production, biomass synthesis, and maintenance of redox balance were shown in 3D culture using sufficient nutrients, which closely resembled the metabolic activity in the xenografts. However, there were several differences between the metabolic activity in the 3D culture and xenografts. In vivo, the cancer tissue had blood flow with stromal cells present around the cancer cells. In the xenografts, we detected metabolized and degraded products in the liver and other organs of the host mice. Furthermore, the 3D system did not show impairment of mitochondrial function in the cancer cells, suggesting that cancer cells produce energy simultaneously through mitochondria, as well as aerobic glycolysis.

## KEYWORDS

cancer metabolism, mitochondrial function, three-dimensional, tissueoid cell culture system, tongue cancer

This is an open access article under the terms of the Creative Commons Attribution NonCommercial License, which permits use, distribution and reproduction in any medium, provided the original work is properly cited and is not used for commercial purposes.

© 2020 The Authors. *Cancer Science* published by John Wiley & Sons Australia, Ltd on behalf of Japanese Cancer Association.

## 1 | INTRODUCTION

It has gradually become clear that mammalian cells grown as conventional two-dimensional (2D) monolayer cultures on rigid and treated surfaces could show different behavior and functional properties from those in the native microenvironment.<sup>1-4</sup> It is speculated that the 3D culture system (hereafter, 3D) might be able to replace animal models.<sup>5</sup> Recently, there have been reports on 3D cancer organoids and cancer tissue-originated spheroids using ECM matter such as spheroids and collagen.<sup>6</sup> We also have recently proposed a novel 3D “tissueoid cell culture system” using Cellbed (Japan Vilene Co.) as a 3D culture carrier.<sup>7,8</sup> Cellbed is a fiber aggregate made of ultrafine silica fiber, and its structure is similar to that of the tissue skeleton of loose connective tissue in a living body.<sup>7,8</sup> Cancer cells can move freely through these voids, creating a 3D structure.<sup>7,8</sup> Furthermore, as only pure cancer cells can be used in this system without an ECM, the system provides the advantage of extracting and analyzing metabolites from pure cancer cells. The tissueoid cell culture system is capable of long-term culture of at least 4 weeks.<sup>7,8</sup>

We produced three groups (2D, 3D using tissueoid cell culture system, and xenografts) using four different types of tongue cancer cell lines. Using the xenografts as the standard, we examined the similarities and differences in metabolites among the three groups. In addition, this study focused on mitochondrial metabolism, which is essential for cancer cell proliferation and tumor development.<sup>9,10</sup>

## 2 | MATERIALS AND METHODS

### 2.1 | Cells and culture

Four types of tongue squamous cell carcinoma cell lines (HSC-3, HSC-4, SCC-4, SCC-15) were purchased from the Japanese Collection of Research Bioresources Cell Bank. HSC-3 and HSC-4 cell lines were established by sampling from cervical lymph node metastatic lesions of a poorly differentiated and a well-differentiated tongue squamous cell carcinoma, respectively.<sup>11</sup> SCC-4 was collected from a primary

lesion of a well-differentiated tongue squamous cell carcinoma that had undergone radiation and chemotherapy prior to sampling.<sup>12</sup> SCC-15 was derived from a primary lesion of a well-differentiated tongue squamous cell carcinoma that was untreated prior to sampling.<sup>12</sup> For both the 2D and 3D cultures, we used DMEM (Nacalai Tesque) for culturing HSC-3 and HSC-4. The medium used for SCC-4 and SCC-15 was DMEM/Ham's F-12 (Nacalai Tesque). Ten percent FBS and 1% antibiotic-antimycotic (ABAM) solution were added to each and 0.4 µg/mL hydrocortisone (TCI) was added to only DMEM/Ham's F-12. We used Cellbed as the 3D culture carrier. The 2D and 3D culture was carried out according to previous reports.<sup>7,8</sup>

### 2.2 | Xenografting experiment

The animal experiments were undertaken with approval from the Animal Experiment Committee of Shiga University of Medical Science (2019-4-1). All cell lines were injected s.c. into the back of 5-week-old male nude mice (BALB/cA-nu/nu). The number of cells injected was  $5 \times 10^6$  cells for HSC-3, SCC-4, and SCC-15, whereas  $1 \times 10^7$  cells were injected for HSC-4. Two weeks subsequent to injection, the mice were killed by cervical dislocation under anesthetic with isoflurane (Wako) overdose. The removed tumors were split into three, and one part was fixed with formalin for H&E staining. The other sections were frozen at  $-80^{\circ}\text{C}$  and subjected to western blot analyses and metabolome analyses.

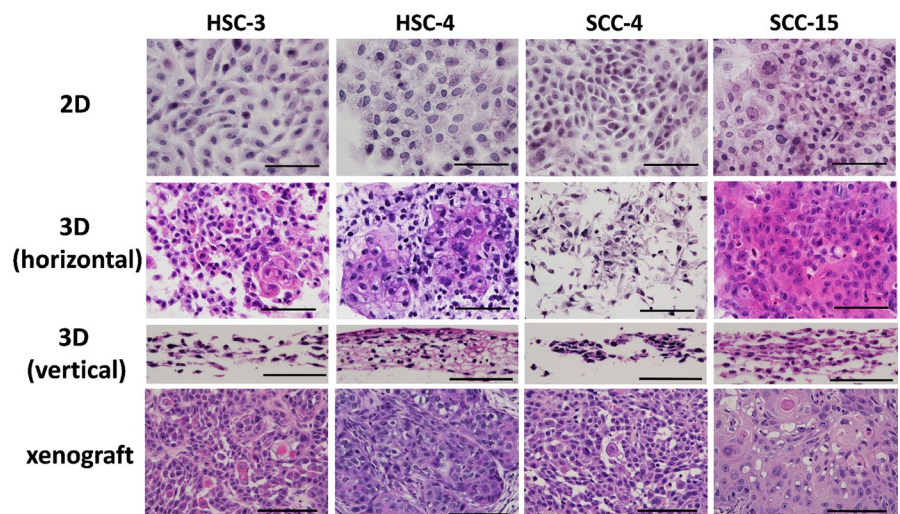
### 2.3 | Hematoxylin-eosin staining

The H&E staining was carried out according to previous reports.<sup>7</sup>

### 2.4 | Metabolome analysis

The 2D culture was established in a 6-cm dish. A separate dish was prepared for cell counting. The 3D system was cultured for 2 weeks.

**FIGURE 1** Histological findings in two-dimensional (2D) and 3D cultures and xenografts of tongue cancer cells (H&E staining; scale bar = 100 µm). In 3D horizontal sections of HSC-4 and SCC-15 cells, abnormal keratinization was detected, and the vertical sections of these cells clearly showed a layered structure. In the xenografts, the nests of HSC-4, SCC-4, and SCC-15 cells were larger than those of HSC-3. Abnormal keratinization was also detected in xenografts



To count the number of cells, MTT assays were carried out the day after seeding, on the day the cells would engraft on the Cellbed. The final number of cells was adjusted so that both 2D and 3D cultures had  $1 \times 10^6$  cells, and the number of cells in the 2D and 3D cultures were unified when later comparing the metabolite levels.

The tumor tissue sections sampled from the xenograft were weighed. The number and weight of cells in the 2D culture was measured in advance, and the number of cells in the xenografts was calculated based on the weight. The weight of the xenografts contained stromal cells; however, as the number of tumor

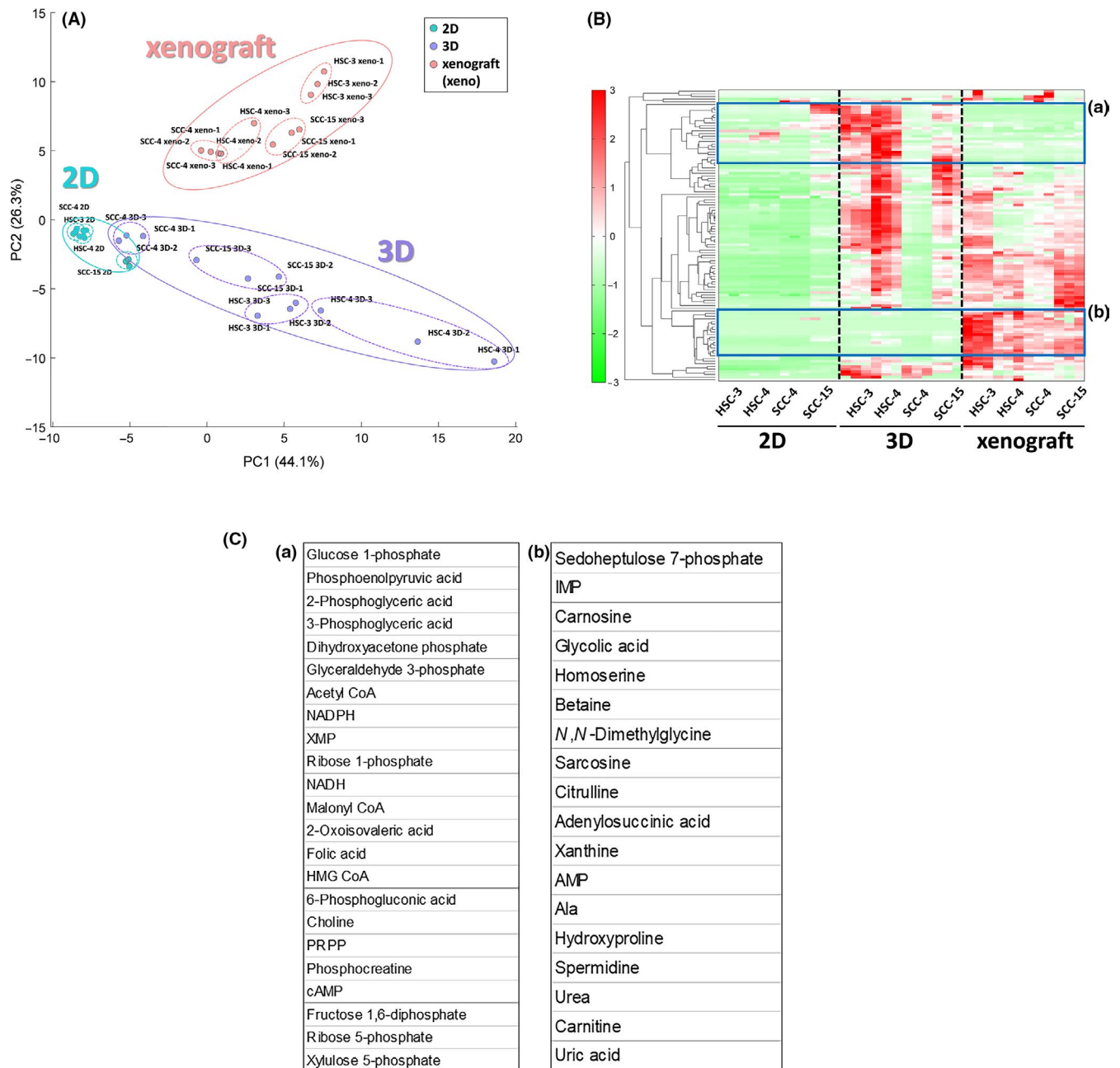


**FIGURE 2** Comprehensive metabolome analysis of two-dimensional (2D) and 3D cultures and xenografts of tongue cancer cells. A, Principal component (PC) analysis. Blue circle, 2D ( $n = 3$ ); purple circle, 3D ( $n = 3$ ); pink circle, xenograft ( $n = 3$ ). In the 2D culture, SCC-15 was in an isolated position, whereas HSC-3, HSC-4, and SCC-4 clustered at approximately the same position. In the 3D and xenograft plots, each cell line has grouped into one position. B, Cluster analysis. Metabolites with low peak intensity only in the xenografts were referred to as (a), and metabolites with high peak intensity only in the xenografts were referred to as (b). Compared to the xenografts, the peak intensity of almost all metabolite peaks in the 2D culture was significantly lower. Conversely, in the 3D, despite the peak intensity being similar to that in the 2D for the SCC-4 cell line, all other cell lines had peaks with similar intensity to those in the xenografts (except Figure 2B(a,b)). C, Lists of metabolites in Figure 2B. (a) Metabolites with low peak intensity in the xenografts were most commonly glycolytic intermediates. (b) Metabolites with high peak intensity in the xenografts were most commonly urea, choline, and purine metabolites of the liver

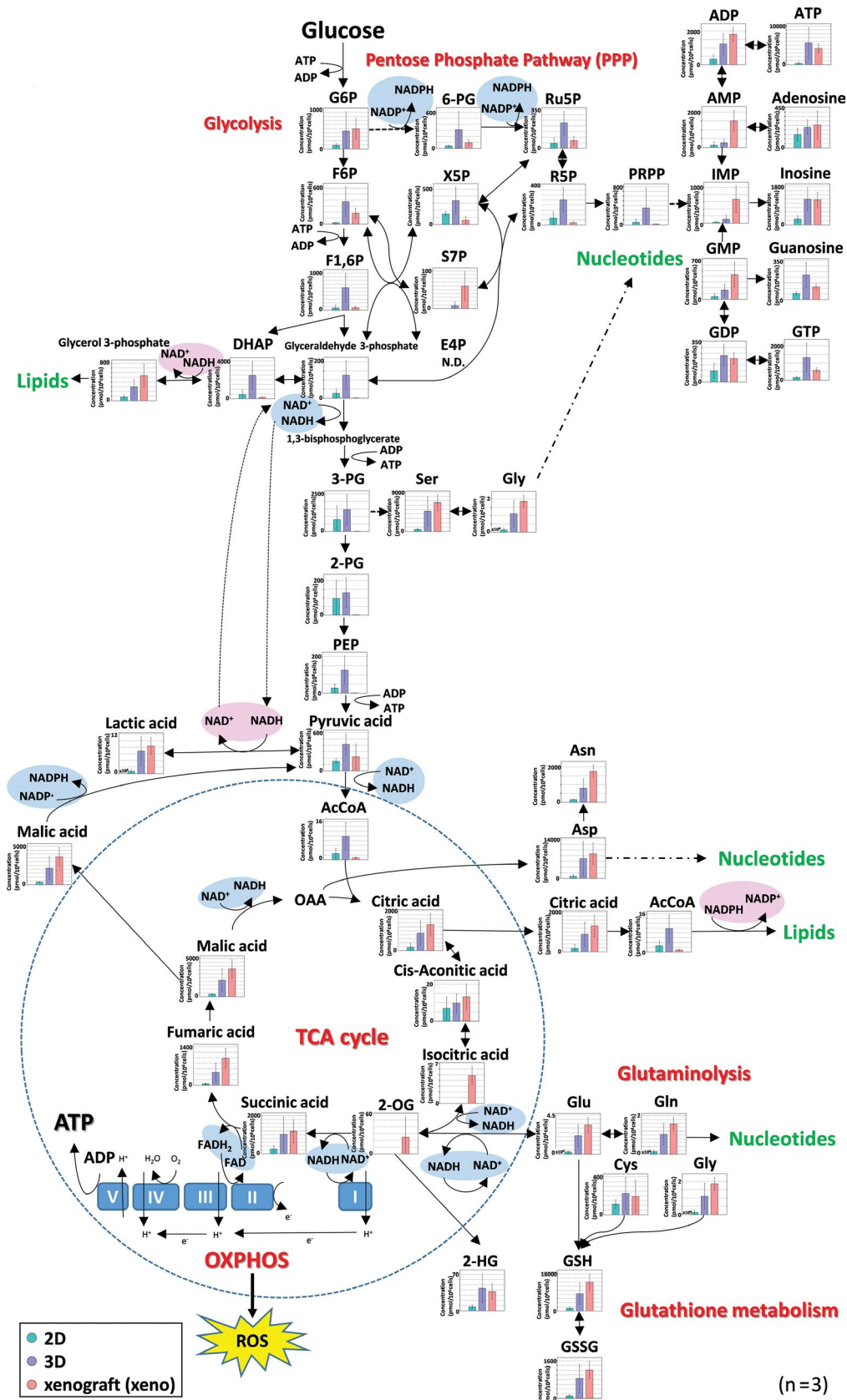


**FIGURE 3** Overview of the metabolic network in two-dimensional (2D) and 3D cultures and xenografts of tongue cancer cells. Nearly all metabolites in the 2D culture were present at levels lower than those in the xenografts. Conversely, several metabolites in the 3D culture were present at levels comparable to those in the xenografts. Metabolites involved in redox balance are shaded in pink (oxidation) and blue (reduction)



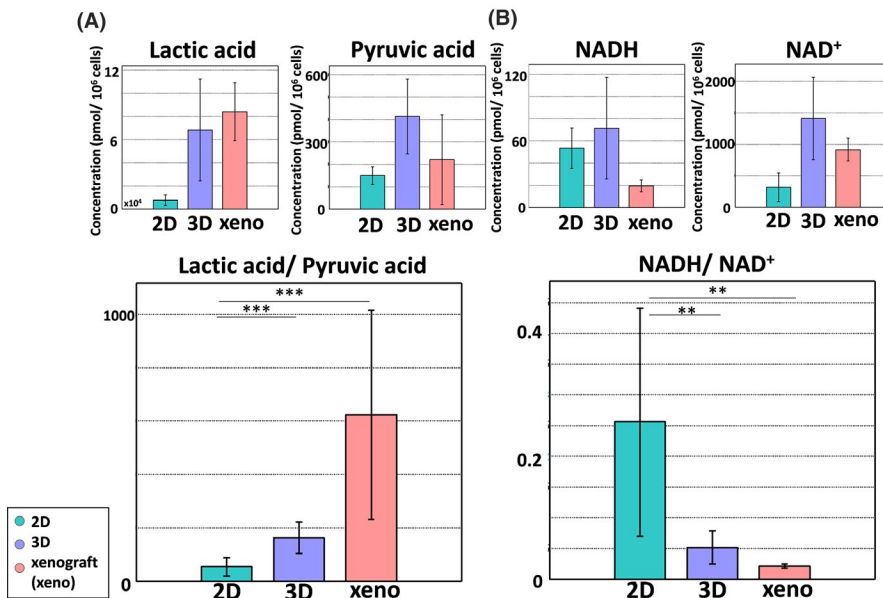


**FIGURE 4** Glycolysis in two-dimensional (2D) and 3D cultures and xenografts of tongue cancer cells. In the 2D, the lactic acid/pyruvate (L/P) ratio was significantly low ( $P = 3.7E-04$ ), while the NADH/NAD<sup>+</sup> ratio was significantly high ( $P = .001$ ). A high quantity of lactic acid was produced in the 3D and the xenografts. ROS, reactive oxygen species

cells was significantly higher than number of stromal cells in the tissue sections sampled, we proceeded to use this method.

Metabolome measurements were undertaken at Human Metabolome Technologies, Inc. The frozen samples were plunged into 50% acetonitrile/Milli-Q water with internal standards (H3304-1002; Human Metabolome Technologies) at 0°C in order to inactivate the enzymes. The tissue was homogenized three times at 1500 rpm for 120 seconds (Micro Smash MS100R; Tomy Digital Biology), and the homogenate was centrifuged at 2300 g and 4°C for 5 minutes. Subsequently, 800  $\mu$ L of the upper aqueous layer was subjected to centrifugal filtration through a Millipore 5-kDa cut-off filter at 9100 g and 4°C for 120 minutes to remove proteins. The filtrate was concentrated in a centrifuge and resuspended in 50  $\mu$ L Milli-Q water for capillary electrophoresis–mass spectrometry (CE-MS) analysis.

## 2.5 | Western blot analysis

The work was carried out according to previous reports.<sup>7</sup> The primary Abs used were succinate dehydrogenase (SDHA) (D6J9M) rabbit mAb (1:1000; Cell Signaling Technology), oxidative phosphorylation (OXPHOS) complex IV subunit I mouse mAb (1:1000, 1D6E1A8; Invitrogen), pyruvate dehydrogenase (C54G1) rabbit mAb (1:1000; Cell Signaling Technology), and superoxide dismutase 2, mitochondrial (SOD2) (D3X8F) rabbit mAb (1:1000, Cell Signaling Technology). The secondary Abs were goat peroxidase-conjugated anti-rabbit IgG (#L3012; Signalway Antibody) and goat peroxidase-conjugated anti-mouse IgG (#AP124P; Millipore). Beta-actin was used as a positive control. The proteins were visualized using HRP substrate and scanned using an enhanced chemiluminescence system (Las 4000; Fuji Film).

## 2.6 | Extracellular flux assays

We used an XF24e extracellular flux analyzer (Seahorse Bioscience) for the oxygen consumption rate (OCR) measurement using the mitochondrial stress test and the glycolytic rate assay. The number of seeded cells was adjusted such that the final cell concentration was  $6 \times 10^4$  cells on the date of measurement. The 2D culture was seeded on a XF24 cell culture plate (Seahorse Bioscience) the day before measurement. The 3D culture was seeded on Cellbed in a 96-well plate 2 weeks before the date of measurement. All cell lines of the 3D culture had the Cellbed transferred to an XF cell plate the day before measurement. The mitochondrial stress test was carried out in an XF base medium containing 10 mmol/L glucose, 1 mmol/L sodium pyruvate, and 2 mmol/L glutamine, and the inhibitors were added by adjusting the final concentration using the XF Cell Mito Stress Test Kit (Seahorse Bioscience) with oligomycin (1.5  $\mu$ mol/L), carbonyl cyanide 4-(trifluoromethoxy)phenylhydrazone (FCCP) (HSC-3, HSC-4, 0.25  $\mu$ mol/L; SCC-4, SCC-15, 0.5  $\mu$ mol/L), and rotenone and antimycin A (R/A; 0.5  $\mu$ mol/L). The glycolytic rate assay was carried out using the XF base medium, without phenol red, and containing 5 mmol/L HEPES, 10 mmol/L glucose, 1 mmol/L sodium pyruvate, and 2 mmol/L glutamine, and the inhibitors were added by adjusting the final concentration to 0.5  $\mu$ mol/L R/A and 50 mmol/L 2-deoxy-glycose. The results were analyzed using WAVE version 2.6.0 (Agilent Technologies).

## 2.7 | Statistical analysis

The statistical analysis for the metabolome analysis was undertaken using Welch's *t* test ( $*P < .05$ ,  $**P < .01$ ,  $***P < .001$ ). Student's *t* test was used for the statistical analysis of other experiments ( $*P < .05$ ,  $**P < .01$ ).

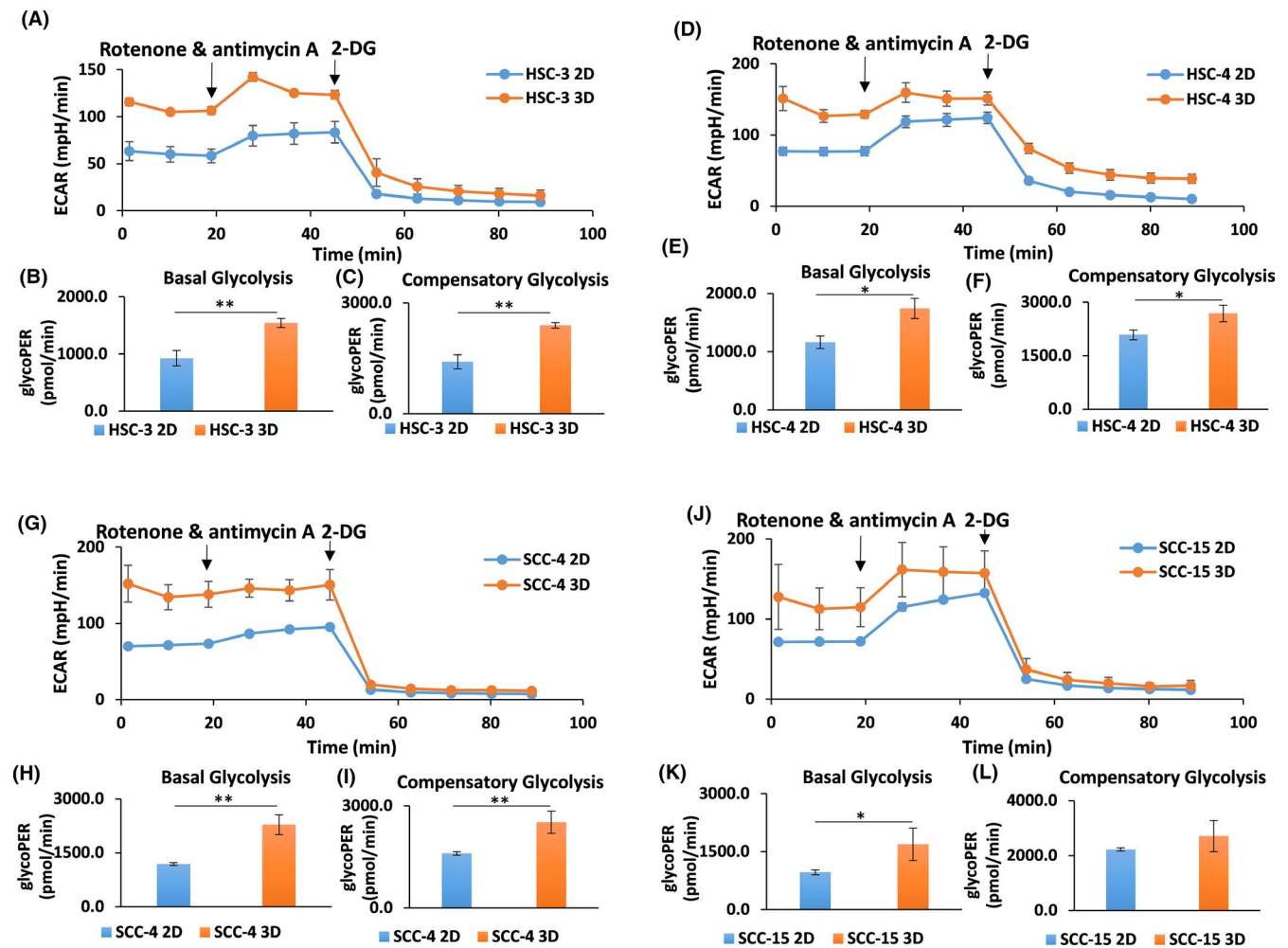


**FIGURE 5** Evaluation of the glycolytic capacity in two-dimensional (2D) and 3D cultures and xenografts of tongue cancer cells using a glycolytic rate kit ( $n = 3$ ). A,D,G,J, Rotenone and antimycin A inhibited mitochondrial respiration, resulting in an increase in the glycoPER, correlated with a complete shift in metabolism from Oxphos to glycolysis. As 2-DG inhibits glycolysis, the efflux rate of protons derived from glycolysis (glycoPER) was reduced. B,E,H,K, In all cell lines, the basal glycolysis levels were significantly higher in the 3D culture than in the 2D. C,F,I,L, In HSC-3, HSC-4, and SCC-4 cells, the compensatory glycolysis levels were significantly higher in the 3D culture than in the 2D.

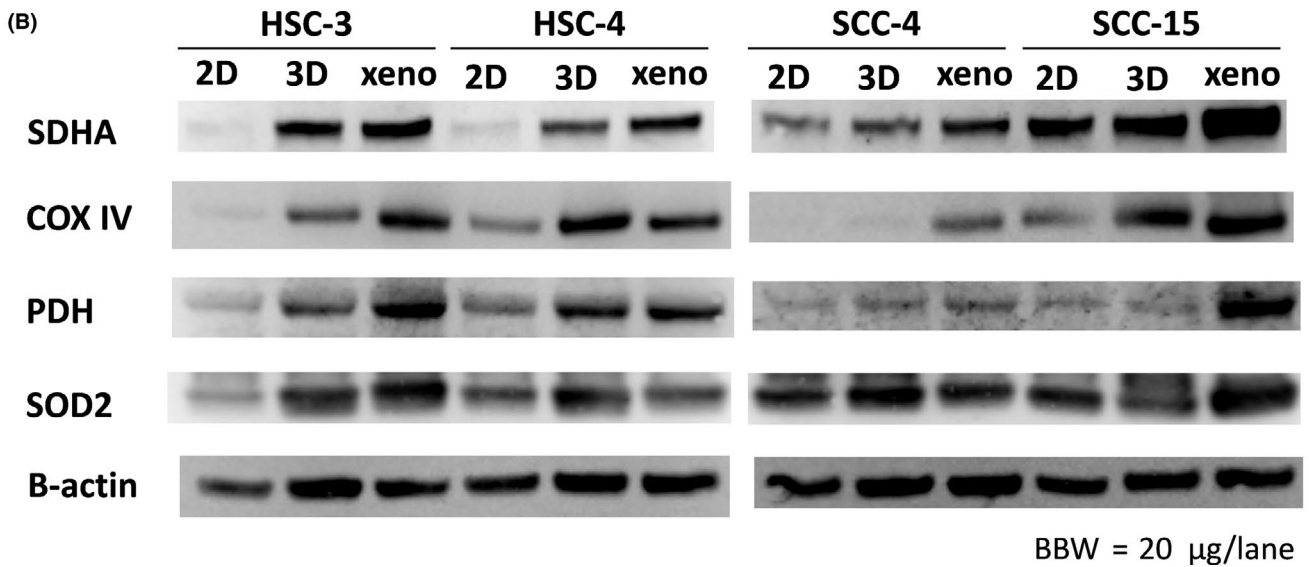
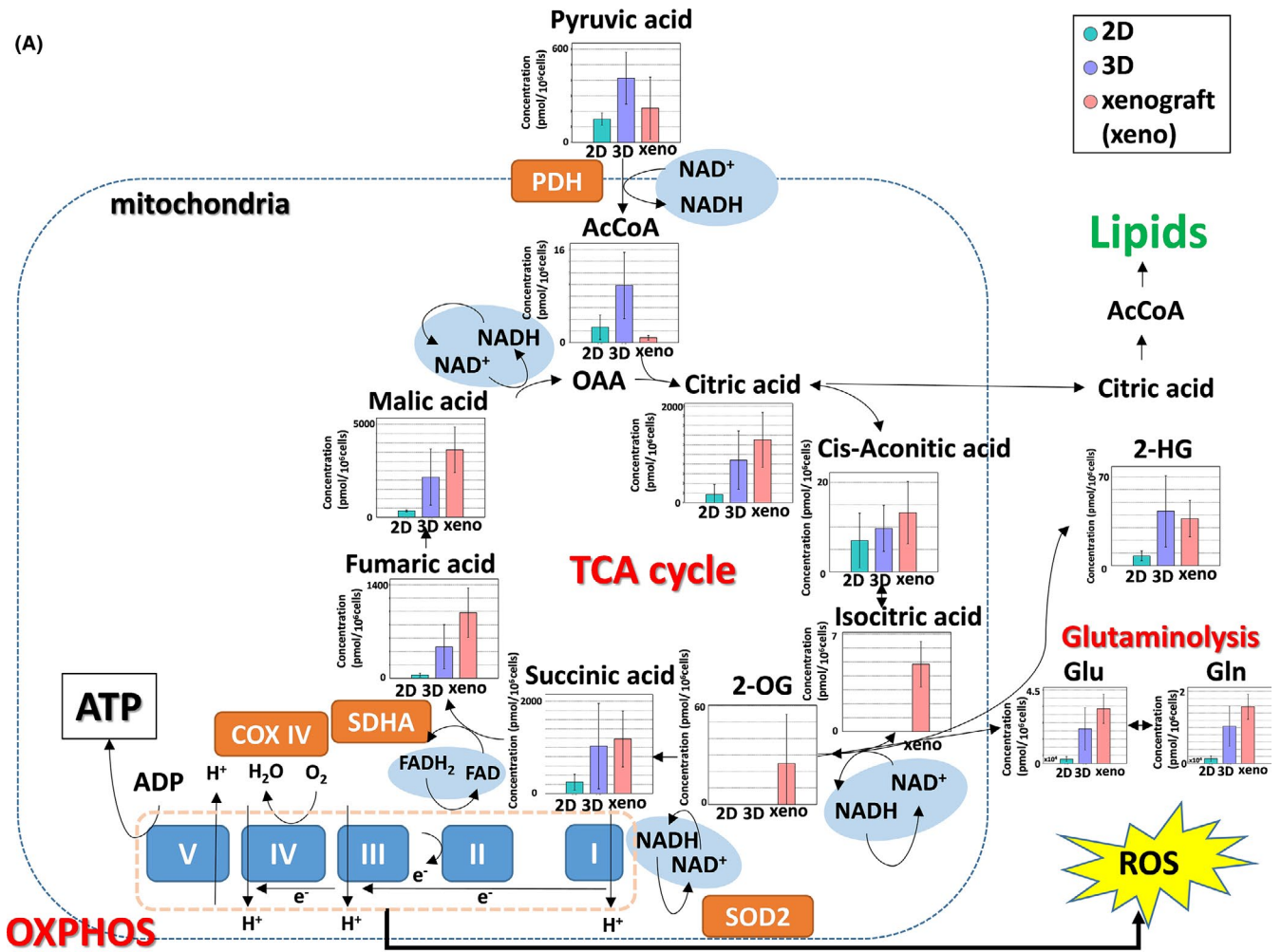
### 3 | RESULTS

#### 3.1 | Hematoxylin–eosin staining of cell lines and xenografts

All cancer cells displayed a monolayer structure in the 2D culture (Figure 1). However, there were differences in the histology of the original site of each cancer cell line in the 3D culture (Figure 1). We clearly

detected abnormal keratinization, a characteristic of squamous cell carcinoma, in 3D horizontal sections of well-differentiated squamous cells without any adjuvant therapy (HSC-4 and SCC-15), and the vertical sections of these cells clearly showed a layered structure. The xenografts showed a sheet-like structure of cancer cells in all cell lines (Figure 1). However, in the xenografts, the nests of HSC-4, SCC-4, and SCC-15 cells were larger than those of the HSC-3 cell line, which was established from a poorly differentiated squamous cell carcinoma (Figure 1).

**FIGURE 6** The TCA cycle and oxidative phosphorylation in mitochondria in two-dimensional (2D) and 3D cultures and xenografts of tongue cancer cells. A, Metabolome analysis of the TCA cycle and oxidative phosphorylation (OXPHOS) in mitochondria. Citric acid, cis-aconitic acid, succinic acid, fumaric acid, and malic acid were present at low levels in the 2D culture, whereas their levels were significantly higher in the 3D and xenografts. B, Western blot analysis of respiratory chain enzymes and reactive oxygen species scavenging enzymes. Expression of both succinate dehydrogenase (SDHA) and complex IV, cytochrome c oxidase (COX IV) was reduced in the 2D culture, whereas the expression levels in the 3D were similar to that in the xenografts. In the 3D culture, the expression levels of COX IV were lower than that of the xenografts only for the SCC-4 cell line. The expression levels of pyruvate dehydrogenase (PDH) and superoxide dismutase 2, mitochondrial (SOD2) were reduced in the 2D culture, whereas their expression levels in the 3D were similar to those observed in the xenografts. Beta-actin is loading control



3.2 | Comprehensive metabolome analysis

The distribution of all cell lines by principal component analysis differed among 2D and 3D cultures and xenografts (Figure 2A). In the

2D culture, while SCC-15 cells were isolated, HSC-3, HSC-4, and SCC-4 cells aggregated to almost the same position. Overall, the 2D culture showed a narrower range of cell line plots compared to the 3D culture and xenografts.

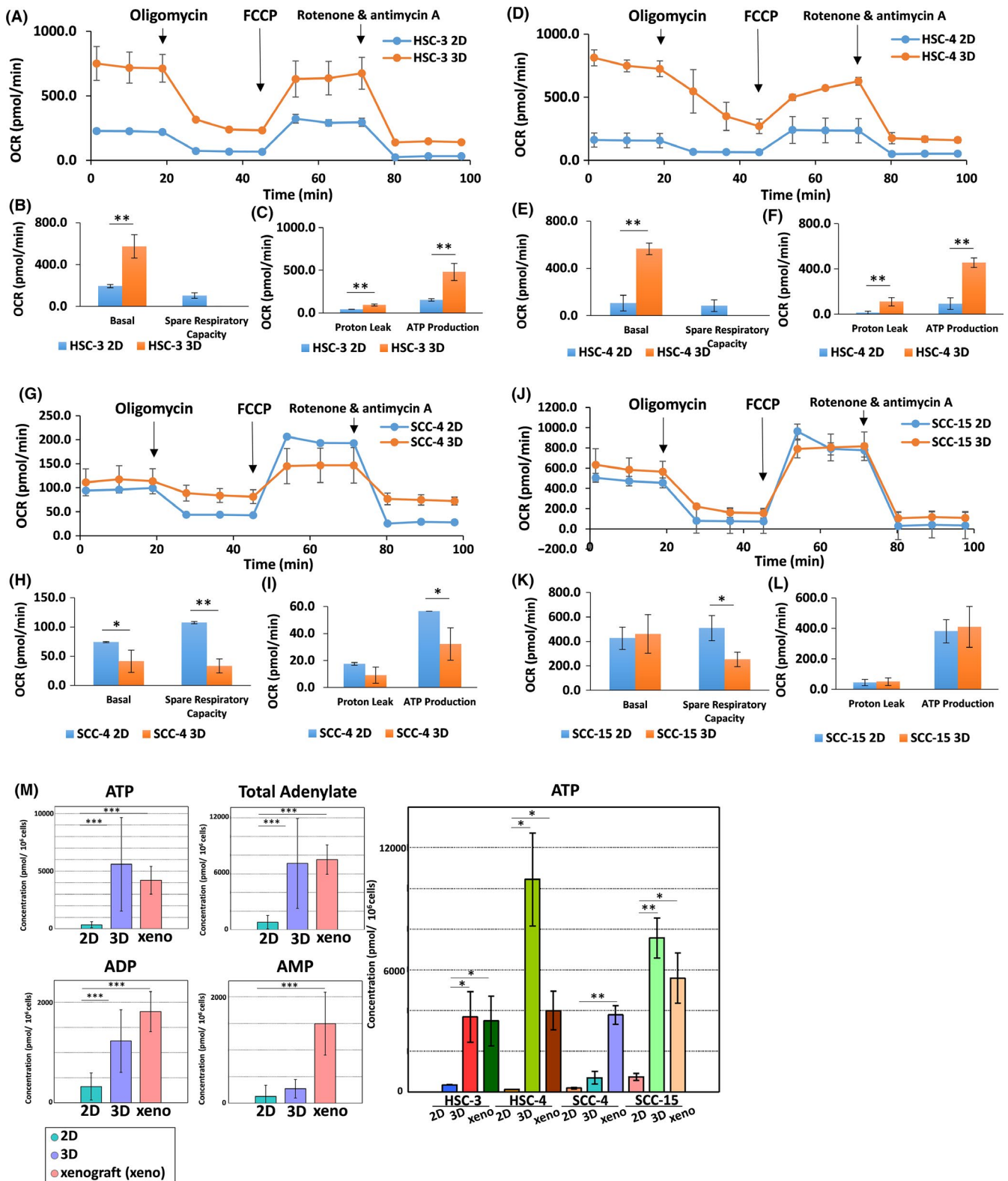


**FIGURE 7** Evaluation of oxidative phosphorylation (OXPHOS) in mitochondria of two-dimensional (2D) and 3D cultures and xenografts of tongue cancer cells using the Mito stress test ( $n = 3$ ). A, D, The oxygen consumption rate (OCR) was higher for 3D than for 2D culture. G, The OCR was no significant differences between SCC-4 2D and SCC-4 3D. J, The OCR was nearly equal between SCC-15 2D and SCC-15 3D. B, C, E, F, In HSC-3 and HSC-4 cell lines, the basal respiratory capacity and ATP production was significantly higher in the 3D culture than in the 2D. In the 3D, the reserve respiratory capacity was 0. H, I, K, L, In the SCC-4 and SCC-15 cell lines, basal respiratory capacity and ATP production did not differ significantly between the 2D and 3D cultures. However, the reserve respiratory capacity in the 3D was significantly lower than that in the 2D. M, The ATP, ADP, AMP, and total adenylate levels were significantly low in the 2D culture, whereas they were mostly comparable between the 3D and xenografts. FCCP, carbonyl cyanide 4-(trifluoromethoxy) phenylhydrazone



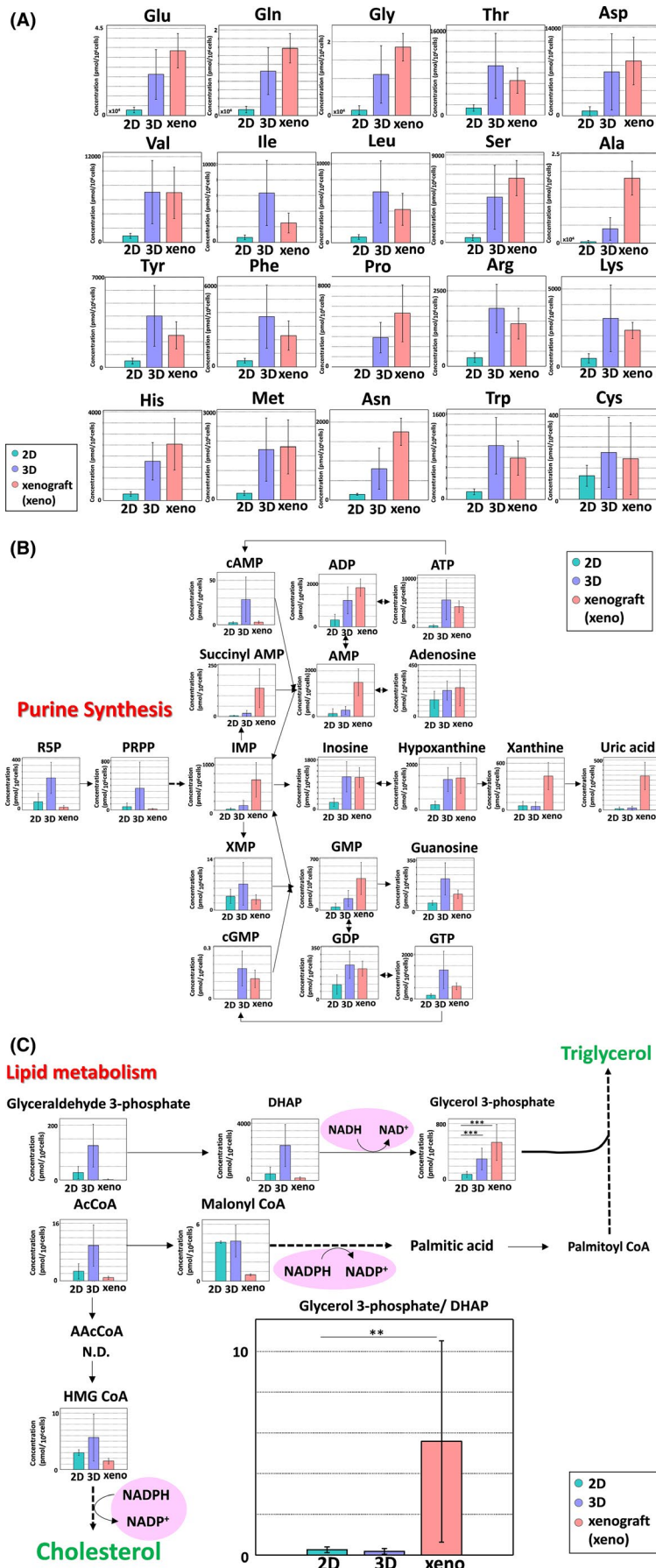


**FIGURE 8** Biomass production in two-dimensional (2D) and 3D cultures and xenografts of tongue cancer cells. A, The quantity of amino acids produced was low in the 2D culture, whereas those in the 3D were high, similar to the xenografts. B, The quantity of purine nucleotides produced in the 2D culture was low, whereas the quantity in the 3D and the xenografts was comparable. Purine base degradation products were present at significantly lower levels in both 2D and 3D cultures compared to the xenografts. C, Acetyl-CoA, later malonyl-CoA and HMG-CoA, were present at high levels in the 3D culture, but their levels were significantly low in the xenografts. There was a significantly lower quantity of glycerol-3-phosphate in the 2D culture than in the xenografts, whereas the amount of glycerol-3-phosphate in the 3D culture was similar to that in the xenografts

We undertook stratified clustering using the metabolites detected and presented the results in the form of a heat map (Figure 2B). Most peaks in 2D were significantly weaker in intensity than those in the 3D and xenografts (Figure 2B). Of the three groups, metabolites with low peak intensity in the xenografts were most commonly glycolytic intermediates (Figure 2B(a)). Conversely, metabolites with high peak intensity in the xenografts were most commonly urea, choline, and purine metabolites of the liver (Figure 2B(b)).

Figure 3 depicts an overview of the metabolic network. Similar to the heat map, the quantities of most metabolites in the 2D culture were significantly lower than in the xenografts. Conversely, the quantities of several metabolites were comparable between the 3D culture and the xenografts.

### 3.3 | Glycolysis

Although the G6P, F6P, F1, 6P, glyceraldehyde-3-phosphate, 3-PG, 2-PG, and PEP metabolite levels were low in the 2D, they were high in the 3D culture (Figure 3). Conversely, the F1, 6P, glyceraldehyde-3-phosphate, 3-PG, 2-PG, and PEP metabolite levels were significantly low in the xenografts (Figure 3). Pyruvic acid is converted to lactic acid using NADH (reduced form) generated by glycolysis, and NAD<sup>+</sup> (oxidized form) during this conversion sustains the flow of the glycolytic. Although the quantity of lactic acid was low in the 2D, it was high in the 3D culture, similar to what was observed in the xenografts (Figure 4). In the 2D, the lactic acid/pyruvic acid ratio was significantly low ( $P = 3.7E-04$ ), whereas the NADH/NAD<sup>+</sup> ratio was significantly high ( $P = .001$ ) (Figure 4).

The glycolytic capacity was evaluated based on the efflux rate of protons derived from glycolysis (glycoPER), using the glycolytic rate test, and comparisons were made between the 2D and 3D. Compared to the 2D, the 3D culture showed higher levels of basal and compensatory glycolysis (Figure 5).

### 3.4 | Metabolomic analysis of TCA cycle and oxidative phosphorylation in mitochondria

The levels of TCA cycle intermediates were low in the 2D culture, but were high in the 3D; similar to that of metabolites in the xenografts, apart from isocitrate and 2-OG levels (Figure 6A). The mitochondria produce ATP by consuming oxygen in the electron transport system, while converting the NADH produced in the TCA cycle to NAD<sup>+</sup> and converting FAD to FADH<sub>2</sub>. During this process, reactive oxygen species (ROS) are produced.<sup>9</sup>

### 3.5 | Western blot analysis of respiratory chain enzymes and ROS scavenging enzymes

Succinate dehydrogenase is an important enzyme involved in the citric acid cycle and oxidative phosphorylation.<sup>13</sup> The electron transport system complex IV, cytochrome c oxidase (COX), is the final enzyme complex in the respiratory chain.<sup>14</sup> The SDHA and COX IV expression levels were low in the 2D culture, whereas those in the 3D culture and xenografts were comparable (Figure 6B). Only the 3D culture of the SCC-4 cell line showed lower expression of COX IV than in the xenografts.

Pyruvate dehydrogenase (PDH), an enzyme that is localized in the mitochondrial matrix, catalyzes the formation of acetyl-CoA from pyruvate in the presence of NAD<sup>+</sup>.<sup>15</sup> Acetyl-CoA is used to produce fatty acids and cholesterol.<sup>15</sup> Expression of PDH was reduced in the 2D culture, whereas the 3D culture had expression levels similar to that in the xenografts (Figure 6B).

Superoxide dismutase 2, mitochondrial (MnSOD), a ROS scavenging enzyme, is a major antioxidant enzyme that catalyzes the conversion of superoxide anion (O<sub>2</sub><sup>-</sup>), a ROS, to hydrogen peroxide and oxygen molecules.<sup>16</sup> Expression of SOD2 was low in the 2D culture. However, the 3D culture had expression levels similar to that of the xenografts (Figure 6B).

### 3.6 | Energy production

We determined the mitochondrial OCR and compared the results between the 2D and 3D cultures (Figure 7A,D,G,J). In the HSC-3 and HSC-4 cell lines, the basal respiratory capacity and ATP production levels were significantly higher in the 3D than in the 2D culture. However, in the 3D culture, the reserve respiratory capacity in the cell lines was 0 (Figure 7B,C,E,F). In the SCC-4 and SCC-15 cell lines, there were no significant differences in the basal respiratory capacity and ATP production levels between the 2D and 3D cultures. However, the reserve respiratory capacity had reduced significantly in the 3D culture in these cell lines (Figure 7H,I,K,L).

The ATP, ADP, AMP, and total adenylate levels were significantly low in the 2D culture; however, they were comparable between the 3D and xenografts (Figure 7M). Comparison of ATP levels revealed that it was significantly low in all cell lines in the 2D culture (Figure 7M). The 3D and xenografts had similar ATP levels for the HSC-3, HSC-4, and SCC-15 cell lines, whereas the 3D culture of the SCC-4 cell line alone had significantly lower ATP levels than the xenografts.

**FIGURE 9** Redox balance in two-dimensional (2D) and 3D cultures and xenografts of tongue cancer cells. A, NADPH is primarily produced in the oxidative processes of the pentose phosphate pathway. B, NADPH protects cells from oxidative stress by eliminating reactive oxygen species (ROS) generated from oxidative phosphorylation. C, The reducing effect of NADPH is important in ROS scavenging as well as in lipid and amino acid syntheses. The NADPH/NADP<sup>+</sup> ratio is low in the 3D culture, similar to that in the xenografts. D, Reduced glutathione (GSH) and oxidized glutathione (GSSG) levels, which exert antioxidant effects, were much higher in both the 3D culture and the xenografts than the 2D culture. SOD2, superoxide dismutase 2, mitochondrial



### 3.7 | Biomass biosynthesis

Amino acid production was low in the 2D culture for amino acids, whereas it was high in 3D and xenografts (Figure 8A).

Purine, a nucleotide, is biosynthesized using ribose 5-phosphate, which is generated in the pentose phosphate pathway (PPP). The levels of purine nucleotides inosinic acid, inosine, AMP, ADP, ATP, adenosine, GMP, GDP, GTP, guanosine, and hypoxanthine were low in the 2D culture, while those in the 3D were similar to that of the xenografts (Figure 8B). The levels of purine degradation products, such as xanthine and uric acid, were significantly lower in both the 2D and 3D cultures compared to in the xenografts (Figure 2B(b)).

The quantity of acetyl-CoA, the starting material for lipogenesis, and that of the subsequently produced malonyl-CoA and HMG-CoA, was high in the 3D culture, but they were significantly low in the xenografts (Figure 8C). As a second pathway of lipid synthesis, glycerol-3-phosphate levels were significantly lower in the 2D culture compared to in the xenografts, whereas those in the 3D were similar to the levels detected in the xenografts (Figure 8C). The glycerol-3-phosphate / DHAP ratio was significantly low in 2D and 3D cultures, whereas it shifted towards biosynthesis of lipids from glycerol-3-phosphate in the xenografts (Figure 8C). Furthermore, the reducing effect of NADPH is important in lipid and amino acid syntheses (Figure 8C).

### 3.8 | Maintenance of redox balance

Nicotinamide adenine dinucleotide phosphate (NADPH) is primarily produced in the processes of the pentose phosphate pathway (Figure 9A). It protects cells from oxidative stress (Figure 9B). The NADPH / NADP<sup>+</sup> ratio in the 3D culture was low, similar to that in the xenografts, which indicated that NADPH was consumed for ROS elimination and biomass biosynthesis (Figure 9C). Furthermore, the glutathione levels were high in the 3D culture for both reduced glutathione (GSH) and oxidized glutathione (GSSG), similar to that in the xenografts (Figure 9D). Reactive oxygen species are intracellular chemical species that contain oxygen and include the superoxide anion (O<sub>2</sub><sup>-</sup>), hydrogen peroxide (H<sub>2</sub>O<sub>2</sub>), and the hydroxyl radical (OH·).<sup>17</sup> The antioxidant enzyme SOD2 catalyzes the conversion of O<sub>2</sub><sup>-</sup> to H<sub>2</sub>O<sub>2</sub> and oxygen. Reduced glutathione reduces H<sub>2</sub>O<sub>2</sub> to H<sub>2</sub>O and becomes oxidized to GSSG.<sup>17</sup> The levels of GSH, GSSG, and total glutathione were high in 3D culture and xenografts (Figure 9D). There was no significant difference in the GSH / GSSG ratio among the three groups (Figure 9D).

## 4 | DISCUSSION

Significant differences in the metabolism of tongue cancer cells between the 2D and 3D cultures were found. Many metabolites in the 3D culture were similar to those in the xenografts. However, because

xenografts are affected by the host stroma surrounding the cancer cells and by blood flow, the affected metabolites differed between cultures. The 3D culture did not impair mitochondrial function in the cancer cells and energy was produced through the mitochondria simultaneously with aerobic glycolysis. Thus, it can be said that cancer cells effectively use oxygen for the biosynthesis of biomass.

The principal component analysis revealed the plots of the four cell lines to be much narrower in 2D culture than in 3D culture and xenograft groups. A previous study reported that metabolic patterns of primary human hepatocytes cultured as conventional 2D monolayers rapidly deteriorated, but the 3D spheroid system is metabolically stable.<sup>18</sup> In this study, the authors detected a peak in AMP levels after 4 hours of 2D culture, suggestive of extensive metabolic remodeling.<sup>18</sup> These results suggested that the characteristics of individual cells were being weakened in the 2D environment and a type of metabolism unique to monolayer culture might be required for survival.

Cancer must undergo metabolic reprogramming that involves synthesizing biomass (nucleotides, amino acids, lipids, and NADPH) from nutrients, which later forms biomaterials and promotes the biosynthesis of macromolecules and organelles.<sup>19,20</sup> In the present study, both the 3D and xenografts showed biosynthesis of high levels of amino acids. Glutamine, in particular, is a substrate for TCA cycle oxidation and a starting material for macromolecular synthesis.<sup>21</sup> Glutamine catabolism is known as "glutaminolysis" and this process is reportedly elevated in several tumors.<sup>9</sup> Our results, especially those shown in Figures 6A and 8A,B, suggested that glutaminolysis was more activated in the 3D culture compared with the 2D culture. Lipids are an essential component of cell membranes and act as signaling molecules as well as energy chargers.<sup>22</sup> De novo fatty acid synthesis is characteristic of cancer cells.<sup>22,23</sup> It was inferred that the acetyl-CoA levels detected in the xenografts were low because the xenografts used acetyl-CoA as a substrate in lipid metabolism. However, as the glycerol-3-phosphate / DHAP ratio was significantly higher in the xenografts than in the 2D and 3D cultures, we surmised that the flux in the xenografts is oriented toward phospholipid synthesis. This suggests that 3D culture and xenografts activate metabolism and produce a large amount of biomass. In contrast, in 2D culture, it was found that biomass production was delayed due to the suppression of metabolic activity.

Mitochondrial metabolism can be considered essential for cancer cell proliferation and carcinogenesis.<sup>24-26</sup> Cancer cells produce most of their ATP through oxidative phosphorylation carried out by the mitochondria.<sup>27,28</sup> In the present study, as the expression levels of respiratory chain enzymes were significantly higher in the 3D culture and xenografts compared with the 2D culture, mitochondrial function was maintained in the 3D culture, much like in the xenografts. Although there were no obvious differences in genomic aberration among the four cell lines (Figure S1), we confirmed that HSC-3 and HSC-4 was more aggressive than SCC-4 and SCC-15 (Figure S2). As a result of OCR measurement, the ATP production by mitochondria in advanced



cancers, which have more aggressive behavior (HSC-3, HSC-4) was significantly higher in the 3D culture than in the 2D culture (Figure S1 and S2). From these results, it can be suggested that 3D culture and xenografts produce a large amount of ATP by activating mitochondrial metabolism, maximizing oxygen utilization, and enhancing the TCA cycle and oxidative phosphorylation in mitochondria.

Cancer cells exposed to oxidative stress activate oxidative PPP, which produces a high quantity of NADPH with increasing ROS levels. In the present study, the NADPH/NADP<sup>+</sup> ratio was significantly lower in the 3D culture and xenografts compared with the 2D culture. Furthermore, as the expression of reactive oxygen species scavenging enzyme (SOD2) was elevated in the 3D culture and xenograft compared with 2D culture, 3D and xenograft consumed a large amount of NADPH made from glucose for ROS scavenging and oxidation. It was suggested that it corresponds to stress. In contrast, in 2D culture, the NADPH / NADP<sup>+</sup> ratio was high and the expression of SOD2 was low, suggesting lower metabolic activity of the ROS elimination system.

Because the 3D culture shows a structure similar to that of in vivo conditions, the interactions between cancer cells were in effect and several metabolites were present at levels that were comparable to those in the xenografts. However, as the in vivo environment maintains blood flow in the cancer tissue, the host metabolites can exert an influence. Thus, the levels of decomposition products of purine nucleotides, such as xanthine and uric acid, decomposition products of the liver, such as urea, and metabolic intermediates of choline to glycine, which are abundant in muscle and body tissues, were high only in the xenografts. From these results, we will try to establish coculture of cancer and stroma cells even in 3D culture in the near future, but we also need to consider the effect of blood flow. However, this 3D tissueoid cell culture system is much better than 2D culture and is expected to be used in a wide range of fields within cancer research.

Based on the present results, unlike in the 3D culture, there were almost no glycolytic intermediates in the xenografts. Although lactic acid, produced by glycolysis, is excreted from cancer cells in the in vivo environment, the lactic acid could be used for angiogenesis and other processes by interaction with the tumor stroma.<sup>29</sup> Additionally, we inferred that cancer cells were reusing lactic acid and converting it to pyruvate before using it in the TCA cycle.

In summary, the cancer cells in the 3D culture and xenografts were shown to actively conduct glycolysis and the citric acid cycle, using nutrients like glucose, for biomass biosynthesis and ATP production by oxidative phosphorylation, as well as to maintain the redox balance. Conversely, the results from the 2D system suggest that a unique form of metabolism was used to enable cell survival under conditions different from the in vivo environment. The 3D metabolome analysis capable of mimicking the morphology and function of in vivo cancer cells yielded results consistent with previously reported theories of cancer metabolism.

## ACKNOWLEDGMENT

We would like to express our gratitude to Mr Takahiro Isono for teaching the technique for extracellular flux assays (Central Research Laboratory, Shiga University of Medical Science). We also thank Mr Takuya Iwasa and Mr Masaaki Kawabe (Japan Vilene Co., Ltd.), who provided information regarding the Cellbed characteristics.

## CONFLICT OF INTEREST

This research was done in collaboration with Japan Vilene Co., Ltd. The company provided Cellbed and information regarding Cellbed materials. Currently, we are applying for seven patents regarding cell observation methods using Cellbed or its peripherals. The authors have no conflicts of interest to declare.

## ORCID

Ken-ichi Mukaisho  <https://orcid.org/0000-0002-0488-0100>

## REFERENCES

1. Tseng H, Gage JA, Shen T, et al. A spheroid toxicity assay using magnetic 3D bioprinting and real-time mobile device-based imaging. *Sci Rep*. 2015;5:13987.
2. Lane AN, Higashi RM, Fan TW-M. Preclinical models for interrogating drug action in human cancers using Stable Isotope Resolved Metabolomics (SIRM). *Metabolomics*. 2016;12:118.
3. Sant S, Johnston PA. The production of 3D tumor spheroids for cancer drug discovery. *Drug Discov Today Technol*. 2017;23:27-36.
4. Ekert JE, Johnson K, Strake B, et al. Three-dimensional lung tumor microenvironment modulates therapeutic compound responsiveness in vitro – implication for drug development. *PLoS ONE*. 2014;9:e92248.
5. Pampaloni F, Reynaud EG, Stelzer EH. The third dimension bridges the gap between cell culture and live tissue. *Nat Rev Mol Cell Biol*. 2007;8:839-845.
6. Kondo J, Endo H, Okuyama H, et al. Retaining cell-cell contact enables preparation and culture of spheroids composed of pure primary cancer cells from colorectal cancer. *Proc Natl Acad Sci USA*. 2011;108:6235-6240.
7. Noi M, Mukaisho KI, Yoshida S, et al. ERK phosphorylation functions in invadopodia formation in tongue cancer cells in a novel silicate fiber-based 3D cell culture system. *Int J Oral Sci*. 2018;10:30.
8. Murakami S, Mukaisho KI, Iwasa T, et al. Application of "tissueoid cell culture system" using a silicate fiber scaffold for cancer research. *Pathobiology*. 2020;87:291-301.
9. Vyas S, Zaganjor E, Haigis MC. Mitochondrial and cancer. *Cell*. 2016;166:555-566.
10. Zong WX, Rabinowitz JD, White E. Mitochondria and cancer. *Mol Cell*. 2016;61:667-676.
11. Momose F, Araida T, Negishi A, Ichijo H, Shioda S, Sasaki S. Variant sublines with different metastatic potentials selected in nude mice from human oral squamous cell carcinomas. *J Oral Pathol Med*. 1989;18:391-395.
12. Rheinwald JG, Beckett MA. Tumorigenic keratinocyte lines requiring anchorage and fibroblast support cultured from human squamous cell carcinomas. *Cancer Res*. 1981;41:1657-1663.
13. Oyedotun KS, Lemire BD. The quaternary structure of the *Saccharomyces cerevisiae* succinate dehydrogenase. Homology modeling, cofactor docking, and molecular dynamics simulation studies. *J Biol Chem*. 2004;279:9424-9431.
14. Kadenbach B, Hüttemann M, Arnold S, Lee I, Bender E. Mitochondrial energy metabolism is regulated via nuclear-coded subunits of cytochrome C oxidase. *Free Radic Biol Med*. 2000;29:211-221.

15. Strumilo S. Short-term regulation of the mammalian pyruvate dehydrogenase complex. *Acta Biochim Pol.* 2005;52:759-764.
16. Cooper ML, Adami HO, Grönberg H, Wiklund F, Green FR, Rayman MP. Interaction between single nucleotide polymorphisms in selenoprotein P and mitochondrial superoxide dismutase determines prostate cancer risk. *Cancer Res.* 2008;68:10171-10177.
17. Lieu EL, Nguyen TU, Rhyne S, Kim J. Amino acids in cancer. *Exp Mol Med.* 2020;52:15-30.
18. Vorrink SU, Ullah S, Schmidt S, et al. Endogenous and xenobiotic metabolic stability of primary human hepatocytes in long-term 3D spheroid cultures revealed by a combination of targeted and untargeted metabolomics. *FASEB J.* 2017;31:2696-2708.
19. Krisher RL, Prather RS. A role for the Warburg effect in preimplantation embryo development: metabolic modification to support rapid cell proliferation. *Mol Reprod Dev.* 2012;79:311-320.
20. Vander Heiden MG, Cantley LC, Thompson CB. Understanding the Warburg effect: the metabolic requirements of cell proliferation. *Science.* 2009;324:1029-1033.
21. DeBerardinis RJ, Mancuso A, Daikhin E, et al. Beyond aerobic glycolysis: transformed cells can engage in glutamine metabolism that exceeds the requirement for protein and nucleotide synthesis. *Proc Natl Acad Sci USA.* 2007;104:19345-19350.
22. Luengo A, Gui DY, Vander Heiden MG. Targeting metabolism for cancer therapy. *Cell Chem Biol.* 2017;24:1161-1180.
23. Currie E, Schulze A, Zechner R, Walther TC, Farese RV Jr. Cellular fatty acid metabolism and cancer. *Cell Metab.* 2013;18:153-161.
24. Joshi S, Tolkunov D, Aviv H, et al. The genomic landscape of renal oncocytoma identifies a metabolic barrier to tumorigenesis. *Cell Rep.* 2015;13:1895-1908.
25. Weinberg F, Hamanaka R, Wheaton WW, et al. Mitochondrial metabolism and ROS generation are essential for Kras-mediated tumorigenicity. *Proc Natl Acad Sci USA.* 2010;107:8788-8793.
26. Martínez-Reyes I, Diebold L, Kong H, et al. TCA cycle and mitochondrial membrane potential are necessary for diverse biological functions. *Mol Cell.* 2016;61:199-209.
27. DeBerardinis RJ, Chandel NS. Fundamentals of cancer metabolism. *Sci Adv.* 2016;2:e1600200.
28. Wallace DC. Mitochondria and cancer. *Nat Rev Cancer.* 2012;12:685-698.
29. Song J, Lee K, Park SW, et al. Lactic acid upregulates VEGF expression in macrophages and facilitates choroidal neovascularization. *Invest Ophthalmol Vis Sci.* 2018;59:3747-3754.

#### SUPPORTING INFORMATION

Additional supporting information may be found online in the Supporting Information section.

**How to cite this article:** Murakami S, Tanaka H, Nakayama T, et al. Similarities and differences in metabolites of tongue cancer cells among two- and three-dimensional cultures and xenografts. *Cancer Sci.* 2021;112:918-931. <https://doi.org/10.1111/cas.14749>